Electrochemical X-Ray Fluorescence Spectroscopy (EC-XRF) for Trace Heavy Metal Analysis: Enhancing XRF Detection Capabilities by Four Orders of Magnitude.

ARTICLE *in* ANALYTICAL CHEMISTRY · APRIL 2014

Impact Factor: 5.64 · DOI: 10.1021/ac500608d · Source: PubMed

6 AUTHORS, INCLUDING:

Tania Louise Read
The University of Warwick
7 PUBLICATIONS **31** CITATIONS
SEE PROFILE

Zoe Ayres
The University of Warwick
2 PUBLICATIONS **8** CITATIONS
SEE PROFILE

Mark Edward Newton
The University of Warwick
105 PUBLICATIONS **1,784** CITATIONS
SEE PROFILE

Julie V Macpherson
The University of Warwick
175 PUBLICATIONS **5,629** CITATIONS
SEE PROFILE

analytical chemistry

Article

pubs.acs.org/ac

Electrochemical X-ray Fluorescence Spectroscopy for Trace Heavy Metal Analysis: Enhancing X-ray Fluorescence Detection Capabilities by Four Orders of Magnitude

Laura A. Hutton,[†,§] Glen D. O'Neil,[†] Tania L. Read,[†] Zoë J. Ayres,[†] Mark E. Newton,*[,‡] and Julie V. Macpherson*[,†]

[†]Departments of Chemistry and [‡]Physics, University of Warwick, Coventry, CV4 7AL, U.K.

[§]Element Six Ltd., Element Six Global Innovations Centre, Harwell Campus, Didcot, OX11 0QR, U.K.

Supporting Information

ABSTRACT: The development of a novel analytical technique, electrochemical X-ray fluorescence (EC-XRF), is described and applied to the quantitative detection of heavy metals in solution, achieving sub-ppb limits of detection (LOD). In EC-XRF, electrochemical preconcentration of a species of interest onto the target electrode is achieved here by cathodic electrodeposition. Unambiguous elemental identification and quantification of metal concentration is then made using XRF. This simple electrochemical preconcentration step improves the LOD of energy dispersive XRF by over 4 orders of magnitude (for similar sample preparation time scales). Large area free-standing boron doped diamond grown using microwave plasma chemical vapor deposition techniques is found to be ideal as the electrode material for both electrodeposition and XRF due to its wide solvent window, transparency to the XRF beam, and ability to be produced in mechanically robust freestanding thin film form. During electrodeposition it is possible to vary both the deposition potential (E_{dep}) and deposition time (t_{dep}). For the metals Cu^{2+} and Pb^{2+} the highest detection sensitivities were found for E_{dep} = −1.75 V and t_{dep} = 4000 s with LODs of 0.05 and 0.04 ppb achieved, respectively. In mixed Cu^{2+}/Pb^{2+} solutions, EC-XRF shows that Cu^{2+} deposition is unimpeded by Pb^{2+}, across a broad concentration range, but this is only true for Pb^{2+} when both metals are present at low concentrations (10 nM), boding well for trace level measurements. In a dual mixed metal solution, EC-XRF can also be employed to either selectively deposit the metal which has the most positive formal reduction potential, E^0, or exhaustively deplete it from solution, enabling uninhibited detection of the metal with the more negative E^0.

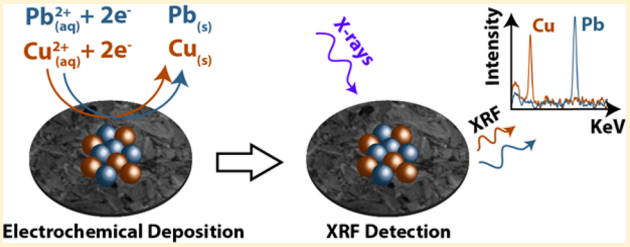

Increasing global industrialization and appreciation of the environmental impact of toxic and carcinogenic chemicals, such as heavy metals, on both humans and wildlife has led to increasingly tighter legislation by government bodies such as the World Health Organization and the U.S. Food and Drug Administration.[1] Regulations require heavy metal quantification to the sub-ppb level in many applications including waste management, pharmaceutical processes, clinical toxicology, and environmental monitoring.[2] The technique used most commonly for heavy metal detection at these levels is inductively coupled plasma mass spectrometry (ICP-MS).[3] However, ICP-MS requires relatively expensive instrumentation, essential sample preparation, and highly trained operators and is not amenable to *in situ* detection. As a result samples must be taken from the source to the laboratory for analysis.[4] In contrast, electrochemical anodic stripping voltammetry (ASV), where dissolved heavy metals are electrochemically reduced on an electrode surface and then subsequently oxidatively stripped, is a much cheaper technique which can be used in the field.[5] ASV was traditionally carried out using liquid mercury (Hg) electrodes, but due to concerns about Hg toxicity alternative (solid) electrodes are now required. Interpretation of ASV stripping peaks using solid electrodes can be challenging, even for single metal systems, due to deposition morphology effecting the number of peaks observed.[6] This is further complicated in multimetal environments where complex interactions during electrodeposition and stripping can cause peak suppression, shifting, and the appearance of intermetallic peaks.[7]

The spectroscopic technique, X-ray fluorescence (XRF) has been utilized for many years for chemical analysis of a wide range of substances from stardust[8] to forensic samples[9,10] providing elemental composition of the material/solution of interest, by virtue of an emitted fluorescence signal. However, while XRF is amenable to *in situ* operation one major drawback has been that detection sensitivity is not sufficient for environmental or pharmaceutical analysis,[11] as it is typically at the ppm level.[12] Several methods have been implemented to improve detection limits including total-reflection (TR) XRF[4a] as well as various preconcentration techniques, such as the use

Received: February 13, 2014
Accepted: April 4, 2014

   dx.doi.org/10.1021/ac500608d | *Anal. Chem.* XXXX, XXX, XXX−XXX

of precipitating agents[13] and controlled evaporation. While these have gone some way to improving sensitivity, the required ppb and lower limits for heavy metals are still unobtainable. An alternative, relatively unexplored method of preconcentration in spectroscopy is electrodeposition. There have been a few examples in the literature, for example, Bulska described the use of electrodeposition for the detection of metals in atomic absorption spectroscopy (AAS),[14] while Tao et al. combined metal electrodeposition and stripping with surface plasmon resonance spectroscopy.[7a] Electrodeposition was also used to improve detection sensitivity for Hg on niobium electrodes in TR-XRF.[15]

In this paper we report the development and application of electrochemical (EC)-XRF as a general analytical technique for the quantitative detection of both single and mixed metal ions solutions over a wide dynamic range from ppm to sub-ppb. We show that the XRF component enables the chemical element to be uniquely identified and quantified via a fluorescence signature, while electrochemical deposition on pBDD electrodes enhances XRF detection sensitivity by over 4 orders of magnitude, compared to traditional energy dispersive (ED)-XRF (with evaporative preconcentration) methodologies. EC-XRF capabilities are illustrated by quantitative sub-ppb detection for Pb and Cu, in both single and mixed metal solutions.

EXPERIMENTAL SECTION

Materials and Solutions. Highly doped, ~3×10^{20} boron atoms cm^{-3}, polycrystalline boron doped diamond (pBDD) electrodes (Element Six Ltd., Harwell, U.K.) 25 mm in diameter, of thicknesses 50 and 250 μm and lapped on the sensing side to rms surface roughness <5 nm, were used as the EC-XRF electrode, as shown in Figure 1a. All solutions were

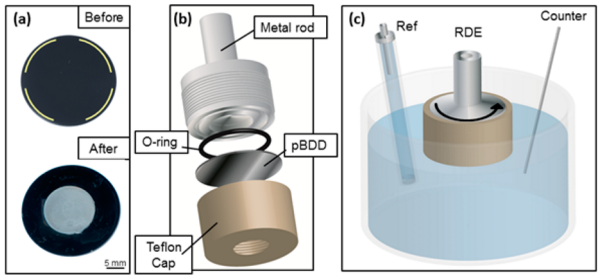

Figure 1. (a) Optical images of the pBDD electrode before and after electrochemical deposition of 10 ppm Pb^{2+} deposited at −1.75 V for 4000 s. Gold on the "before" image indicates the location of the Ti/Au contacts on the backside of the pBDD disk. (b) Deconstructed rotating disc arrangement and (c) experimental setup for electrochemical deposition using a pBDD rotating disc electrode.

prepared from Milli-Q water (Millipore Corp.), resistivity 18.2 MΩ cm at 25 °C. The redox mediator hexaammineruthenium-(III) chloride $(Ru(NH_3)_6^{3+}$ (Strem Chemicals, Newbury Port, MA) was used to investigate the electrochemical characteristics of the pBDD electrode.[6] Heavy metal salts of lead(II) nitrate ($Pb(NO_3)_2$, 99.999%, Aldrich), copper(II) nitrate ($Cu(NO_3)_2$, 99.999%, Aldrich), and cadmium(II) nitrate ($Cd(NO_3)_2$, 99.999%, Aldrich) were dried and kept in a desiccator prior to solution preparation. Potassium nitrate (KNO_3, 99.999%, Fisher Scientific) was used as the supporting electrolyte for all electrodepositions at a concentration of 1 mM in order to prevent ohmic drop.

XRF. XRF analysis was carried out using an ED-XRF (NEX CG, Rigaku, Japan). The X-ray tube with Pd anode was run at 50 kV with a 1 mA current, using both Mo ($K\alpha$ = 17.48 keV) and Cu ($K\alpha$ = 8.05 keV) secondary targets, selected to ensure optimal excitation of the element of interest. After electrodeposition, the pBDD disk (Figure 1a) was removed from the working electrode setup (Figure 1b) and placed in the XRF with the deposition side facing the X-ray source. All spectra were measured under moderate vacuum (12 Pa) for a sampling time of 300 s. The interrogation area of the X-ray source is elliptical and ~1.2 cm in diameter, in the widest part. Electrochemical preconcentration strategies were compared against Rigaku patented evaporative methodology (Ultra Carry), consisting of a plastic sample plate containing an X-ray transmissive, hydrophobic film with a central absorbent pad. In brief, 200 μL of the solution of interest was placed on the central pad of the Ultra Carry and heated on a hot plate (IKA RCT Basic) at 45 °C until all solution had evaporated, which typically took ~60 min. XRF analysis was then carried out. All XRF spectra were background corrected and filtered using a Savitsky-Golay filter (unless stated otherwise).[16]

Electrochemical Setup. For electrochemical deposition, the pBDD electrode was connected as the RDE working electrode in a three electrode configuration as shown in Figure 1c; Pt gauze was used as the counter electrode and a saturated calomel electrode (SCE) as the reference electrode. All potentials are quoted versus SCE, unless otherwise stated. An ohmic contact to the electrode was made by sputtering a ring of 10 nm Ti/400 nm Au (2.2 cm inner diameter) on the backside of the pBDD through a mask and annealing at 400 °C for 5 h. The ring is carefully positioned to avoid any interference with the X-rays during analysis, as illustrated in Figure 1a. The electrode disc was then screwed in place between a Teflon cap, an O-ring, and metal rod (Figure 1b), the latter of which was part of a commercial rotating disk (Oxford Electrodes, U.K.), to create an electrical connection. The O-ring sealed Teflon cap provided a water-tight seal and reduced the solution accessible pBDD disk to a diameter of 1.4 cm. The electrode was then placed, inverted, into the solution of interest, as shown in Figure 1c.

Electrochemical Deposition. All electrochemical measurements were made in a three-electrode mode using a potentiostat (CHI730A, CH Instruments Inc., TX) connected to a laptop computer. The laboratory was air conditioned to 23 ± 1 °C for all measurements. Metal electrodeposition was performed at rotation speeds of 20 Hz, in 50 mL of solution, with the electrode held at a defined potential for a known period of time. Prior to each deposition, the electrode was freshly cleaned using alumina polish (0.05 μm sized particles, Micropolish, Buehler, Germany) on a water saturated polishing pad (Microcloth, Buehler) and then polished using a dry, clean polishing pad in order to remove any alumina particles. This latter procedure has previously been demonstrated by X-ray photoelectron spectroscopy to rid the surface of alumina particles.[6] The electrodes were gently rinsed using deionized water after deposition, and prior to spectral analysis, to remove excess salt crystals from the supporting electrolyte.

Experimental Design. In order to validate the use of EC-XRF as an analytical technique, a full factorial experimental design approach was taken for the vast majority of EC-XRF experiments carried out. The variables investigated included (1) applied potential, E_{dep}, −0.30 V, −0.55 V, −1.00 V, and −1.75 V versus SCE; (2) electrodeposition time, t_{dep}, 1000 s, 2000 s,

dx.doi.org/10.1021/ac500608d | Anal. Chem. XXXX, XXX, XXX−XXX

and 4000 s; (3) total concentration of Pb^{2+} and Cu^{2+} in the system, 10, 100, and 1000 nM; and (4) ratio of Cu^{2+}/Pb^{2+}, 0:1, 1:1, 1:3, 3:1, 1:0. In total, 180 EC-XRF experiments were carried out in a randomized order as listed in the Supporting Information, section 1 so as not to induce bias into the measurements. A total of 29 extra repeat experiments were built into the design at random intervals to investigate reproducibility in the measurement (Supporting Information, section 1).

RESULTS AND DISCUSSION

Freestanding pBDD wafers are an excellent choice for an electrode substrate in EC-XRF due to (i) BDD's wide solvent window and high overpotential for hydrogen production;[17] (ii) B and C are noninterfering elements in the XRF spectrum; the elemental range for XRF is Na to U; and (iii) the substrate can be lapped flat (<5 nm roughness) and thinned.[18] However, it was first important to ascertain the thickness of pBDD suitable for use in XRF analysis. Figure 2a shows the background

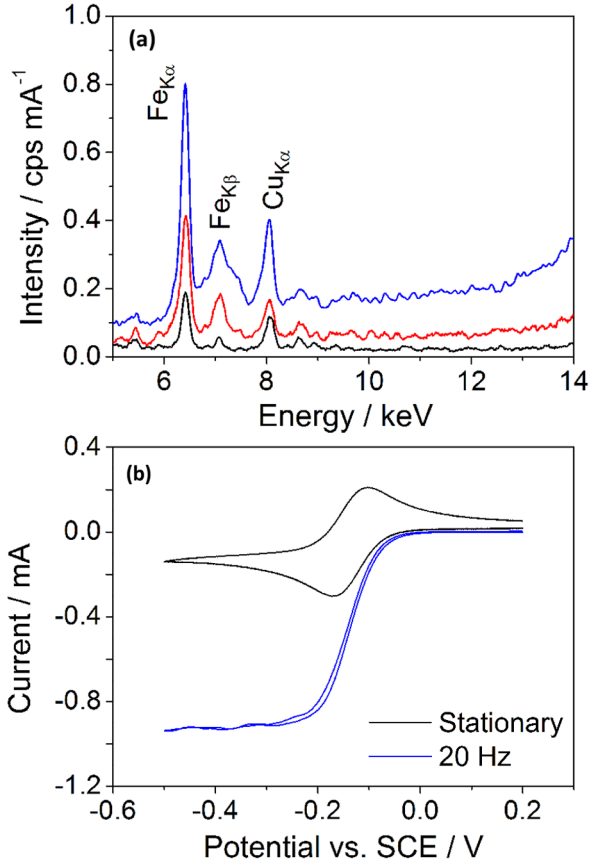

Figure 2. (a) XRF background spectra with (i) Ultra Carry (black); (ii) 50 μm pBDD (red); and (iii) 250 μm pBDD (blue) in the sample chamber. Note these spectra are not background corrected or filtered. (b) Electrochemical characterization for the reduction of 1 mM $Ru(NH_3)_6^{3+}$ in 0.1 M KNO_3 at a scan rate of 0.1 V s^{-1}, in stationary (black) solution and rotated (blue) at 20 Hz.

fluorescence spectra for pBDD electrodes of 50 μm (red line) and 250 μm thickness (blue line), compared against the Ultra Carry (black line). As can be seen, background fluorescence is influenced by pBDD thickness, with the signal rising as the thickness increases due to increased X-ray scatter. Although the 50 μm thick pBDD fluorescence signature compares well with that of the Ultra Carry, the 250 μm electrode is mechanically more robust and easier to handle. As this electrode only has a slightly larger background fluorescence, all experiments were performed using this electrode. For all traces in Figure 2a, both Cu and Fe peaks are observed, these are attributed to residual scattered X-rays from the brass shutter and the steel body of the sample chamber fluorescing close to the optical path. All EC-XRF spectra were thus background corrected using a representative blank sample.

In order to ensure that the 25 mm diameter disk of pBDD was suitably doped to function efficiently as an electrode, especially as the electrode diameter (1.4 cm) is larger than electrodes typically used in electroanalysis, the electrochemical response was investigated using $Ru(NH_3)_6^{3+}$ ($E_{1/2}$ of −0.11 V versus SCE).[6,18] Figure 2b shows the CV response for the reduction of 1 mM $Ru(NH_3)_6^{3+}$ in 0.1 M KNO_3 at a scan rate of 0.1 V s^{-1}. Close to reversible behavior is observed, with a peak to peak (ΔE_p) separation of 65 mV, indicative of highly doped "metal-like" diamond material. This value also shows there is good electrical connection to the pBDD, and ohmic drop, either across the solution or substrate, is minimal; especially important considering the high currents passed. The peak current, i_p = 0.35 mA, is close to that expected theoretically (0.39 mA, Randles Sevcik theory)[19] assuming a diffusion coefficient, D, for $Ru(NH_3)_6^{3+}$ of 8.8×10^{-6} cm^2 s^{-1} [20] and the number of electrons transferred per redox event is one.

For an electrode of this size in quiescent solution, diffusion of analyte to the surface is slow. In order to increase mass transport and reduce deposition times, forced convection was implemented by rotating the electrode. The CV response for the reduction of 1 mM $Ru(NH_3)_6^{3+}$ in 0.1 M KNO_3 at a scan rate of 0.1 V s^{-1} and rotation rate, f, of 20 Hz is also shown in Figure 2b. Because of the increased mass transport, the current now attains a steady-state with a limiting value of 0.92 mA. This value is close to that predicted by Levich theory for the rotation rate employed (0.95 mA),[19] as shown in the Supporting Information, section 2. Because of the design of the electrode holder, the experimental limiting currents deviate away from Levich behavior at higher rotation rates (Supporting Information, section 2); therefore, all subsequent electrodepositions were carried out at f = 20 Hz.

To highlight the advantage of electrochemical preconcentration using EC-XRF, traditional ED-XRF was compared against EC-XRF for a solution containing 10 nM (0.64 ppb) Cu^{2+}. In the former, solution was evaporated onto the Ultra Carry substrate (60 min) while in the latter electrodeposition was carried out at E_{dep} = −1.75 V, on the pBDD electrode for 2000 s (33.3 min, just over half the time required for evaporation). Figure 3a shows the $Cu_{K\alpha}$ XRF spectra for the two different substrate preparation methods. Importantly a clear peak of intensity 0.97 cps mA^{-1} at 8.05 keV (Cu signal) is observed in EC-XRF, for the subpbb Cu^{2+} solution, while no detectable signal is observed for the evaporation-only XRF approach. The increase in signal is due to electrodeposition and hence preconcentration of Cu at the surface of the BDD electrode, highlighting the advantages of EC-XRF over XRF for trace-level measurements. Moreover, XRF brings to electrochemical analysis the ability to uniquely identify, by virtue of the observed keV for fluorescent emission, the elemental identity of the species in solution.

Furthermore, electrochemical preconcentration also has the advantage that it can significantly increase measurement selectivity in a solution matrix by eliminating interfering species that are not electroactive. This is essential in the analysis of

dx.doi.org/10.1021/ac500608d | Anal. Chem. XXXX, XXX, XXX−XXX

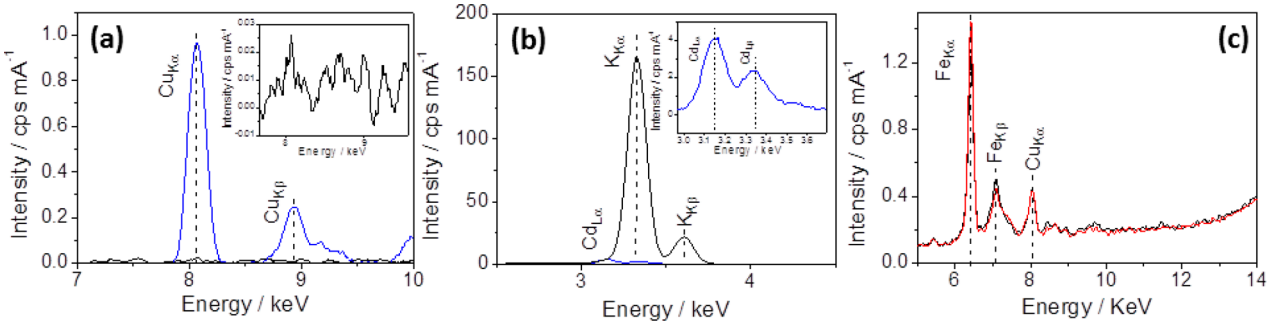

Figure 3. XRF spectra of (a) 10 nM Cu^{2+} solution and (b) 4.5 μM Cd^{2+} in 1 mM KCl solution, using the Ultra Carry (black) and pBDD (blue), the latter collected using E_{dep} = −1.75 V and t_{dep} = 4000 s. (c) Background XRF spectra for pBDD substrate before (black) and after 10 repeated depositions and cleaning steps (red), E_{dep} = −1.75 V.

complex mixtures and is illustrated in Figure 3b, which shows XRF spectra for a solution containing 4.5 μM (0.5 ppm) Cd^{2+} (in 1 mM KCl) recorded using both evaporative (Ultra Carry, black line) and electrodeposition (blue line) preparative methods (E_{dep} = −1.75 V and t_{dep} = 4000 s). The XRF emission lines for Cd^{2+} ($Cd_{L\alpha}$ line at 3.13 keV) and K^+ ($K_{K\alpha}$ line at 3.31 keV) are closely spaced. With the evaporative procedure, as K^+ is higher in concentration by almost 3 orders of magnitude it is therefore impossible to resolve the Cd^{2+} signature. This is a problem in XRF environmental analyses where K^+ is often a major component of the solution matrix.[21] Note the $Cd_{K\alpha}$ peak at 23.17 keV was not used for identification purposes due to the poor excitation efficiency. In contrast, when EC-XRF is employed, only species that can be electrochemically deposited in the solvent of interest are detected, as shown in the inset to Figure 3b. Consequently EC-XRF enables the Cd signal to be clearly resolved in solutions containing high amounts of background contaminants, again highlighting the advantage of electrochemical preconcentration and EC-XRF.

In order to use the pBDD electrode reproducibly and repeatedly, it was important to verify the electrode could be cleaned such that all electrodeposited metals could be removed from the surface post-analysis. Figure 3c shows the background fluorescence spectra of a pristine pBDD disk prior to electrodeposition (black) and after 10 electrodeposition experiments (red). In between every experiment, the pBDD electrodes were cleaned by alumina polishing. The two signals are nearly identical, within error, which shows that the cleaning procedure adopted is effective at removing deposited metals allowing for consistent background measurements to be obtained from experiment to experiment.

In order to investigate whether EC-XRF could be used quantitatively, the effect of E_{dep} and t_{dep} were investigated for single metal Cu^{2+} and Pb^{2+} solutions of a fixed concentration. Figure 4 shows the effect of different E_{dep} (−0.55 V, −1 V, and −1.75 V) and t_{dep} (1000 s, 2000 s, and 4000 s) on the XRF signals for solutions containing (a) 100 nM (6.4 ppb) Cu^{2+} and (b) 100 nM Pb^{2+} (20.7 pbb) in 1 mM KNO_3 (pH = 6.5). The E_{dep} values were chosen to provide a wide range of different driving forces for metal electrodeposition. Note, on pBDD, due to water reduction being strongly retarded, there is minimal current flowing even at −1.75 V (Supporting Information, section 3); although once electrodeposition takes place the metal will provide electrocatalytic sites for hydrogen evolution. However, bubble formation was never observed during

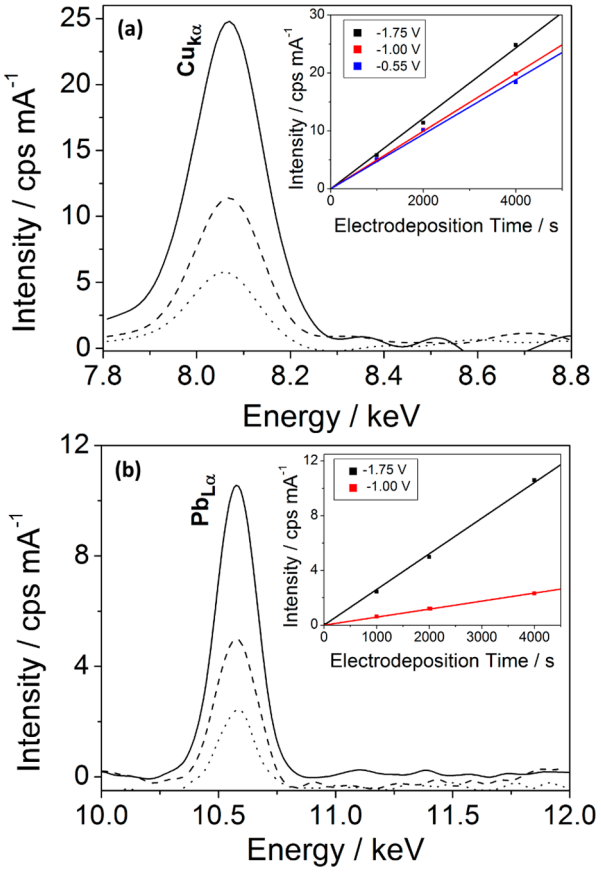

Figure 4. EC-XRF spectra for 100 nM (a) Cu^{2+} and (b) Pb^{2+}, with E_{dep} = −1.75 V and t_{dep} = 1000 s (dotted), 2000 s (dashed), and 4000 s (solid). Inset: Plots of EC-XRF peak intensities versus t_{dep} for 100 nM (a) Cu^{2+} and (b) Pb^{2+} and E_{dep} of −0.55 V (blue), −1 V (red), and −1.75 V (black).

experiments, even for the most extreme conditions employed (E_{dep} = −1.75 V and t_{dep} = 4000 s).

Parts a and b of Figure 4 show the $Cu_{K\alpha}$ (8.05 keV) and $Pb_{L\alpha}$ (10.56 keV) peaks, respectively, at the largest applied E_{dep} = −1.75 V, for t_{dep} of 1000 s (dotted), 2000 s (dashed), and 4000 s (solid). A clear linear correlation of deposition time with EC-XRF peak intensity is observed for both metals (insets in Figures 4a,b) with a gradient of 0.051 ± 0.002 cps mA^{-1} s^{-1} (R^2 = 0.999) and 0.0026 ± 0.0001 cps mA^{-1} s^{-1} (R^2 = 0.999) for Cu and Pb, respectively, at −1.75 V. Note even though the CV shown in the Supporting Information, section 4, indicates an

dx.doi.org/10.1021/ac500608d | Anal. Chem. XXXX, XXX, XXX−XXX

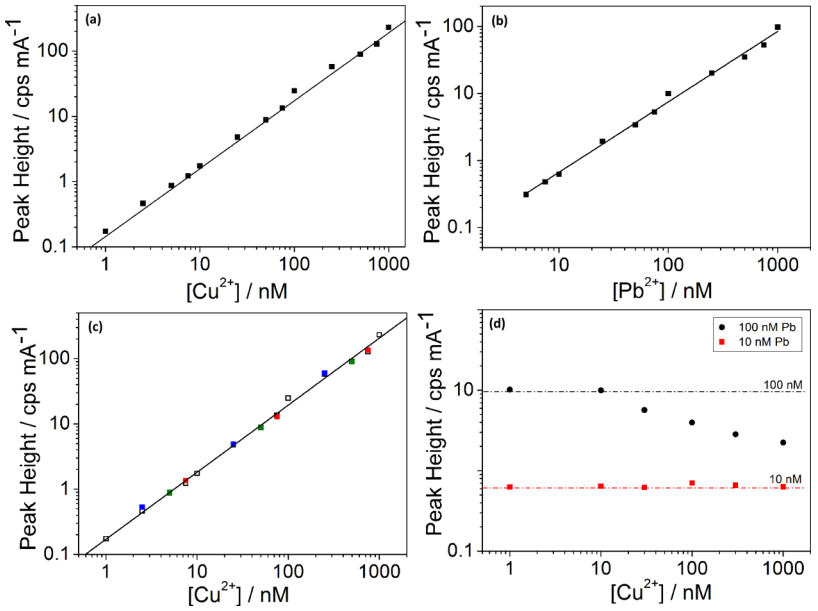

Figure 5. Plots of concentration vs EC-XRF peak height for E_{dep} = −1.75 V and t_{dep} = 4000 s for single-metal (a) Cu^{2+} and (b) Pb^{2+} solutions. (c) The effect of [Pb^{2+}] on EC-XRF peak height for Cu^{2+} detection in mixed-metal solutions for concentration ratios blue ■, 1:3 Cu/Pb; green ■, 1:1 Cu/Pb; and red ■, 3:1 Cu/Pb. Also plotted are the single-metal Cu^{2+} data (□) for comparison. (d) The effect of [Cu] on the Pb EC-XRF peak heights in mixed metal solutions. [Pb^{2+}] is fixed at 10 nM (red ■) and 100 nM (●) and [Cu^{2+}] varied.

$E_{1/2}$ of −0.07 V vs SCE for Cu electrodeposition on pBDD, E_{dep} = −0.3 V was found insufficient to deposit Cu at detectable levels in EC-XRF, even for t_{dep} = 4000 s. However, for E_{dep} = −0.55 V, −1.00 V, and −1.75 V, the intensity of the $Cu_{K\alpha}$ line increased as E_{dep} increased. For Pb, at E_{dep} values of −0.3 V and −0.55 V no XRF signal for Pb Lα was seen, in accordance with the CV shown in Figure S3b in the Supporting Information, section 4 ($E_{1/2}$ = −0.7 V), where no current flows at these potentials. As E_{dep} was increased from −1.00 V to −1.75 V, the gradient increased from 5.9 (±0.1) × 10^{-4} cps mA^{-1} s^{-1} (R^2 = 0.998) to 0.0026 ± 0.0001 cps mA^{-1} s^{-1} (R^2 = 0.999), respectively. For the highest sensitivity signals for both Cu and Pb it is thus preferable to use the highest driving force for electrodeposition, i.e., E_{dep} = −1.75 V.

To explore this further, the XRF signal dependence on concentration was investigated for E_{dep} = −1.75 V where the signal intensity is highest. Figure 5 shows plots of peak height versus solution concentration for (a) Cu^{2+} and (b) Pb^{2+} over the concentration range 1 nM (0.06 ppb [Cu] and 0.2 ppb [Pb]) to 1000 nM (60 ppb [Cu] and 200 ppb [Pb]) for a fixed t_{dep} and E_{dep} of 4000 s and −1.75 V, respectively. For Cu, the gradient of the line is 1.04 ± 0.02 cps mA^{-1} nM^{-1} (R^2 = 0.995) giving a limit of detection (LOD; 3σ) of 0.75 nM (0.05 ppb) for Cu using a measured noise intensity of 0.1 cps mA^{-1}. For Pb, the gradient of the line is 1.05 ± 0.02 cps mA^{-1} nM^{-1} (R^2 = 0.999), which gives a LOD of 1.8 nM (0.04 ppb). It is possible to further decrease limits of detection by simply increasing deposition time, as is shown in Figure 4. Using the XRF evaporative method (Ultracarry) and typical evaporative times of 3600 s, LODs for Cu and Pb of only 0.27 ppm and 0.18 ppm, respectively, were calculated, as described in the Supporting Information, section 5. EC-XRF thus enables an improvement in LOD by 4 orders of magnitude for similar time scales. It is important to note that the replicate measurements built into the experimental design all show a very high degree of repeatability, compared to the initial measurement (for Cu and Pb more than half the repeats were within 2% and 3% of each other, respectively; Table S2, Supporting Information, section 1).

It is also of interest to consider the EC-XRF response in mixed metal solutions. Figure 5c,d shows the EC-XRF response for solutions containing Cu^{2+} and Pb^{2+}. As for Figure 5a,b, E_{dep} and t_{dep} were fixed at −1.75 V and 4000 s, respectively. In Figure 5c, the total concentration of metal was kept constant at either 10 nM, 100 nM, or 1000 nM; however, the ratio of the two metals was varied. For example, a 1:1 total concentration of 100 nM contains 50 nM Cu^{2+} and 50 nM Pb^{2+}. XRF signals of the single metal ion of known concentration were directly compared with that from the mixed metal solution. Figure 5c shows a plot of Cu^{2+} concentration versus peak intensity when present in mixed metal solutions (blue ■, 1:3 Cu/Pb; green ■, 1:1 Cu/Pb; red ■, 3:1 Cu/Pb). Peak intensities for Cu from single metal solutions are also plotted for reference (□). Figure 5c shows that the EC-XRF signal for Cu^{2+} from mixed-metal deposits falls on the calibration line of the Cu^{2+} only plot. This observation indicates that the electrodeposition of Cu is unaffected by the presence of Pb in solution, even when the Pb is in excess (Cu/Pb ratio 1:3, blue ■).

An analogous set of experiments was performed using the signal from the Pb Lα line (data not shown) which indicated that at certain concentration ratios of Pb/Cu the Pb XRF signal deviated from the line for Pb alone. In order to investigate this observation further, it was necessary to carry out more detailed experiments beyond the original scope of the experimental design work program. EC-XRF experiments were thus recorded in mixed metal solutions where the concentration of Pb was kept constant (10 nM, red ■) and (100 nM, ●) and the Cu concentration was increased from 1 nM to 10 nM, 30 nM, 100 nM, 300 nM, and 1000 nM, as shown in Figure 5d. E_{dep} and t_{dep} were fixed at −1.75 V and 4000 s, respectively. In Figure 5d, the dashed horizontal lines represent the peak height observed for solutions containing only 10 nM or 100 nM Pb^{2+} electrodeposited at −1.75 V and 4000 s. Interestingly, for 10 nM Pb^{2+}, the Pb XRF peak height signal stays the same irrespective of the

dx.doi.org/10.1021/ac500608d | Anal. Chem. XXXX, XXX, XXX−XXX

amount of Cu^{2+} in the mixture, with (Cu/Pb) ratios of 1:10; 1:1; 3:1; 10:1; 30:1, and 100:1. When the amount of Pb^{2+} is increased 10-fold, the Pb XRF signature is unaffected by the presence of Cu for (Cu/Pb) ratios of (1:100) and (1:10); however, even when the Pb is still 3.33 times in excess of the Cu, the Pb XRF peak height signature has now decreased below that for a Pb only solution (43% decrease). The Pb XRF peak signature decreases even more as the concentration of Cu in the mixture is increased from (1:1, 60% decrease); (3:1, 71% decrease); and (10:1, 78% decrease).

The XRF results indicate that for this two component mixture (Pb/Cu), the metal which is deposited under the higher driving force (largest overpotential), here Cu, electrodeposits independently of the concentration of the second metal, Pb, over the concentration range investigated. We are currently investigating to see whether this is a general observation for any two (or higher) component metal mixtures. For Pb, however, the amount of metal deposited was affected by the concentration of Cu in solution and the relative concentration ratio. For low Pb concentrations (10 nM, 2.1 ppb) the amount of Pb electrodeposited on the surface appeared independent of the amount of Cu in solution (over 3 orders of magnitude Cu concentration range 1 nM−1 μM). However, simply increasing the Pb concentration to 100 nM resulted in the amount of Pb depositing on the surface decreasing as the concentration of Cu increased beyond ≥30 nM. The data suggests that Cu electrodeposition under certain conditions impedes Pb electrodeposition. The fact that no impediment is observed at very low concentrations suggests that particles of Pb and Cu are able to nucleate independently on the surface and bodes well for the use of EC-XRF as an analytical tool for low ppb measurements in mixed metal solutions. However, as the concentration of Pb increases, competition of the two metals for available surface sites and possible Pb−Cu interactions suppresses Pb nucleation, compared to a Pb only solution of the same concentration. We are currently investigating these observations in more detail using high-resolution microscopic techniques to observe metal nucleation morphologies at various stages of the electronucleation process.

Because of the complicated nature of codeposition of different metals for quantitative analysis, especially at higher concentrations, it may be preferable to either selectively electrodeposit the metal of interest or exhaustively remove the interfering metal from solution. As E_{dep} is an experimental variable in EC-XRF, both are possible, as demonstrated by the data in Figure 6 for a solution containing 10 nM (0.6 ppb) Cu^{2+} and 10 nM (2.1 ppb) Pb^{2+}. As shown by the black trace, a judicious choice of E_{dep} (−0.55 V) means it is possible to selectively deposit Cu from the two metals mixture, (t_{dep} = 1000 s).

The red trace shows the EC-XRF data after exhaustive depletion of Cu from solution. Here the pBDD substrate was held at E_{dep} = −0.55 V for a sufficiently long time, t_{dep} = 5000 s, in order to electrodeposit all the Cu^{2+} from solution onto the electrode. Qualitatively t_{dep} was determined from knowledge of the number of moles of Cu^{2+} in solution, n_{mol}, where $t_{dep} = n_{mol}F/i$, and i was estimated from the current flowing under Levich conditions for the known concentration of Cu^{2+}. The sample volume was decreased to 20 mL in order to decrease t_{dep}. A clean pBDD electrode was then employed for electrodeposition of Pb from the Cu^{2+} depleted solution (E_{dep} = −1.75 V and t_{dep} = 2000 s). The red trace in Figure 6 clearly shows no Cu in the spectra indicating exhaustive depletion of Cu. The Pb peak intensity is in close agreement with the linear calibration data in Figure 5b for 10 nM Pb^{2+} in a single metal solution.

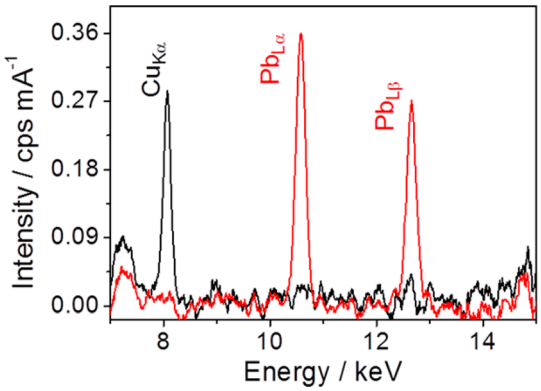

Figure 6. EC-XRF spectra for 10 nM Cu^{2+} and 10 nM Pb^{2+} solution after (i) deposition at −0.55 V for 1000 s (black) and (ii) exhaustive depletion of Cu^{2+} from solution (−0.55 V for 5000 s) and deposition of Pb^{2+} onto a clean pBDD substrate at −1.75 V for 2000 s (red).

Finally it is of interest to compare the merits of EC-XRF against more traditional XRF and ASV. We have shown that by using electrochemical deposition it is possible to enhance detection sensitivities for metal ions in solution using (ED)-XRF alone by 4 orders of magnitude. In ASV, for a single metal system although a single peak is expected which scales in height or area with concentration,[22] the situation is complicated by deposition morphology affecting the number of stripping peaks observed. Hence for an unknown system, multiple peaks could lead the researcher to assume multiple metals present.[23,24] For mixed metal systems, ASV interpretation is further complicated. For example, for the Pb/Cu system, conflicting ASV data has been reported in the literature. Some report enhancement of the Pb signal in the presence of Cu[7b,25] while others document the opposite.[26] For solid electrodes, between two to four peaks have been seen in Pb/Cu ASVs, ascribed to various different redox processes,[7b,25a,26] e.g., (i) Pb oxidation to Pb^{2+}; (ii) Cu oxidation to Cu^{2+}; (iii) Cu oxidation to Cu^{+}; (iv) intermetallic Cu−Pb oxidation; and (v) hydrogen evolution on Cu nuclei (under low pH conditions), making analytical quantification of the data very challenging. This is further complicated if the measurements are carried out in solutions where the chemical identity of redox species is unknown. Moreover, it is also important to consider ASV only reflects material that has been oxidatively stripped from the surface during the potential scan and may not represent all the metal nucleated on the surface.

In contrast, EC-XRF, by virtue of the fluorescence signature, is able to uniquely identify the elemental identity of any metal electrodeposited on the surface, boding well for measurements in real environments. It is also able to quantify how much metal is nucleated on the surface. Further work will now look to assess the potential benefits of using EC-XRF alongside ASV and microscopy to provide a detailed understanding of metal reduction and oxidation processes in mixed metal systems and assessment of the validity of peak assignment in ASV for complex solutions.

CONCLUSION

A hybrid analytical technique for trace metal analysis, combining electrochemical deposition on pBDD and XRF,

dx.doi.org/10.1021/ac500608d | Anal. Chem. XXXX, XXX, XXX−XXX

has been described for the first time. Electrodeposition is used to preconcentrate metal ions from solution onto the surface of a conducting diamond electrode while XRF is used to identify the metal and quantify how much is on the surface. BDD is employed as the electrode material due to its wide potential window, mechanical robustness, ability to be prepared in thin freestanding samples, and its low X-ray scattering cross section. Using an experimental design approach, the effect of E_{dep}, t_{dep}, metal concentration, and metal ratio (for mixed metal systems) were investigated. The most sensitive LODs were reported for E_{dep} = −1.75 V and t_{dep} = 4000 s, where a linear relationship between XRF peak height and metal concentration was observed over the range 1 nM−1 μM for Cu^{2+} (LOD = 0.05 ppb) and Pb^{2+} (LOD = 0.04 ppb). These LODs are 4 orders of magnitude lower than using conventional energy dispersive XRF over similar time scales, for sample preparation.

Mixed-metal systems (Cu and Pb) were investigated in order to provide insight into the use of EC-XRF in more complex environments. EC-XRF data showed that at high driving potentials (E_{dep} = −1.75 V) deposition of the metal with the more positive half wave potential (i.e., Cu^{2+}) was unaffected by the presence of the second species (Pb^{2+}), across a wide concentration range (1 nM−1 μM). For Pb, however, this was valid only when both metals were present at low (10 nM) concentrations, which bodes well for trace level analysis. It was also possible using EC-XRF to exhaustively remove the metal with the most positive formal potential from solution, enabling the unimpeded deposition and measurement of the second species. In principle, any metal which can be reduced onto the surface of the electrode will be able to quantitatively assessed using EC-XRF. We envisage the future use of algorithms (where deposition potential is a controlled variable) to routinely analyze unknown mixed metal solution. Furthermore, electrochemical preconcentration also has the advantage that it can significantly increase measurement selectivity in a solution matrix by eliminating interfering species that are not electroactive, something evaporative preparative techniques cannot do.

Finally, future work is directed at (i) taking this methodology from the lab bench into the real environment for *in situ* analysis of a wide range of heavy metals in environmental applications and (ii) the real-time understanding of metal growth and dissolution processes by coupling this methodology with high-resolution microscopy and anodic stripping voltammetry.

■ ASSOCIATED CONTENT

Supporting Information

(1) Experimental design and replicate data; (2) electrochemical characterization of the rotating EC-XRF BDD electrode in $Ru(NH_3)_6^{3+}$; (3) EC-XRF BDD electrode solvent window in potassium nitrate solution; (4) CVs of Cu^{2+} and Pb^{2+} electrodeposition and stripping on pBDD; and (5) Ultra Carry XRF calibration for Cu^{2+} and Pb^{2+}. This material is available free of charge via the Internet at http://pubs.acs.org.

■ AUTHOR INFORMATION

Corresponding Authors

*E-mail: m.e.newton@warwick.ac.uk.
*E-mail: j.macpherson@warwick.ac.uk.

Notes

The authors declare no competing financial interest.

■ ACKNOWLEDGMENTS

We would like to thank Element Six for funding (L.A.H. and G.D.O.) and providing the polished thin diamond electrodes used herein (Dr. Tim Mollart and Nicola Palmer), Jonathan Newland (Department of Chemistry, Warwick) for taking the images used in Figure 1a, and Dr. John Fenlon (Department of Statistics, Warwick) for assistance with the experimental design program of work.

■ REFERENCES

(1) Yang, S.; Zhou, D.; Yu, H.; Wei, R.; Pan, B. *Environ. Pollut.* **2013**, *177*, 64−70.
(2) Deibler, K.; Basu, P. *Eur. J. Inorg. Chem.* **2013**, *2013*, 1086−1096.
(3) (a) Bersier, P. M.; Howell, J.; Bruntlett, C. *Analyst* **1994**, *119*, 219−232. (b) Aragay, G.; Pons, J.; Merkoçi, A. *Chem. Rev.* **2011**, *111*, 3433−3458.
(4) (a) Stoessel, R. P.; Prange, A. *Anal. Chem.* **1985**, *57*, 2880−2885. (b) Badiei, H. R.; Liu, C.; Karanassios, V. *Microchem. J.* **2013**, *108*, 131−136.
(5) Ugo, P.; Moretto, L. M.; Vezzà, F. *ChemPhysChem* **2002**, *3*, 917−925.
(6) Hutton, L. A.; Iacobini, J. G.; Bitziou, E.; Channon, R. B.; Newton, M. E.; Macpherson, J. V. *Anal. Chem.* **2013**, *85*, 7230−7240.
(7) (a) Wang, S.; Forzani, E. S.; Tao, N. *Anal. Chem.* **2007**, *79*, 4427−4432. (b) Babyak, C.; Smart, R. B. *Electroanalysis* **2004**, *16*, 175−182.
(8) Silversmit, G.; Vekemans, B.; Brenker, F. E.; Schmitz, S.; Burghammer, M.; Riekel, C.; Vincze, L. *Anal. Chem.* **2009**, *81*, 6107−6112.
(9) Nakano, K.; Nishi, C.; Otsuki, K.; Nishiwaki, Y.; Tsuji, K. *Anal. Chem.* **2011**, *83*, 3477−3483.
(10) West, M.; Ellis, A. T.; Potts, P. J.; Streli, C.; Vanhoof, C.; Wegrzynek, D.; Wobrauschek, P. *J. Anal. At. Spectrom.* **2013**, *28*, 1544−1590.
(11) Campbell, I.; Xiao, Y.; Vrebos, B.; Kempenaers, L.; Coler, D.; Macchiarola, K. *Use of EDXRF for Pharmaceutical Material Elemental Analysis*; white paper, 2010
(12) Melquiades, F. L.; Appoloni, C. R. *J. Radioanal. Nucl. Chem.* **2004**, *262*, 533−541.
(13) (a) Alvarez, A. M.; Alvarez, J. R. E.; Alvarez, R. P. *J. Radioanal. Nucl. Chem.* **2000**, *245*, 485−489. (b) Linder, H. R.; Seltner, H. D.; Schreiber, B. *Anal. Chem.* **1978**, *50*, 896−899.
(14) Bulska, E. *Pure Appl. Chem.* **2001**, *73*, 1−7.
(15) Ritschel, A.; Wobrauschek, P.; Chinea, E.; Grass, F.; Fabjan, C. *Spectrochim. Acta, Part B: At. Spectrosc.* **1999**, *54*, 1449−1454.
(16) Savitzky, A.; Golay, M. J. E. *Anal. Chem.* **1964**, *36*, 1627−1639.
(17) (a) Luong, J. H. T.; Male, K. B.; Glennon, J. D. *Analyst* **2009**, *134*, 1965−1979. (b) Swain, G. M.; Ramesham, R. *Anal. Chem.* **1993**, *65*, 345−351.
(18) Wilson, N. R.; Clewes, S. L.; Newton, M. E.; Unwin, P. R.; Macpherson, J. V. *J. Phys. Chem. B* **2006**, *110*, 5639−5646.
(19) Bard, A. J.; Faulkner, L. R. *Electrochemical Methods: Fundamentals and Applications*; John Wiley and Sons: New York, 2001.
(20) Macpherson, J. V.; O'Hare, D.; Unwin, P. R.; Winlove, C. P. *Biophys. J.* **1997**, *73*, 2771−2781.
(21) Stosnach, H. *Spectrochim. Acta, Part B: At. Spectrosc.* **2006**, *61*, 1141−1145.
(22) Tercier, M. L.; Buffle, J. *Electroanalysis* **1993**, *5*, 187−200.
(23) Hutton, L. A.; Newton, M. E.; Unwin, P. R.; Macpherson, J. V. *Anal. Chem.* **2011**, *83*, 735−745.
(24) Ward Jones, S. E.; Chevallier, F. G.; Paddon, C. A.; Compton, R. G. *Anal. Chem.* **2007**, *79*, 4110−4119.
(25) (a) Prado, C.; Wilkins, S. J.; Marken, F.; Compton, R. G. *Electroanalysis* **2002**, *14*, 262−272. (b) Gunasingham, H.; Dalangin, R. R. *Anal. Chim. Acta* **1991**, *246*, 309−313.
(26) Fierro, S.; Watanabe, T.; Akai, K.; Yamanuki, M.; Einaga, Y. *J. Electrochem. Soc.* **2011**, *158*, F173−F178.